ACS Chemical Neuroscience
Cite This: ACS Chem. Neurosci. 2018, 9, 578−586
Research Article
pubs.acs.org/chemneuro

Development of a Positron Emission Tomography Radiotracer for Imaging Elevated Levels of Superoxide in Neuroinflammation

Catherine Hou,[†] Chia-Ju Hsieh,[†] Shihong Li,[†] Hsiaoju Lee,[†] Thomas J. Graham,[†] Kuiying Xu,[†] Chi-Chang Weng,[†] Robert K. Doot,[†] Wenhua Chu,[‡] Subhasish K. Chakraborty,[§] Laura L. Dugan,[§] Mark A. Mintun,[‡] and Robert H. Mach*[,†]

[†]Department of Radiology, Perelman School of Medicine, University of Pennsylvania, Philadelphia, Pennsylvania 19104, United States
[‡]Mallinckrodt Institute of Radiology, Washington University School of Medicine, St. Louis, Missouri 63110-1016, United States
[§]Department of Medicine, Vanderbilt University School of Medicine, Nashville, Tennessee 37232, United States

ABSTRACT: Reactive oxygen species (ROS) are believed to play a major role in the proinflammatory, M1-polarized form of neuroinflammation. However, it has been difficult to assess the role of ROS and their role in neuroinflammation in animal models of disease because of the absence of probes capable of measuring their presence with the functional imaging technique positron emission tomography (PET). This study describes the synthesis and in vivo evaluation of [^{18}F]ROStrace, a radiotracer for imaging superoxide in vivo with PET, in an LPS model of neuroinflammation. [^{18}F]ROStrace was found to rapidly cross the blood−brain barrier (BBB) and was trapped in the brain of LPS-treated animals but not the control group. [^{18}F]*ox*-ROStrace, the oxidized form of [^{18}F]ROStrace, did not cross the BBB. These data suggest that [^{18}F]ROStrace is a suitable radiotracer for imaging superoxide levels in the central nervous system with PET.

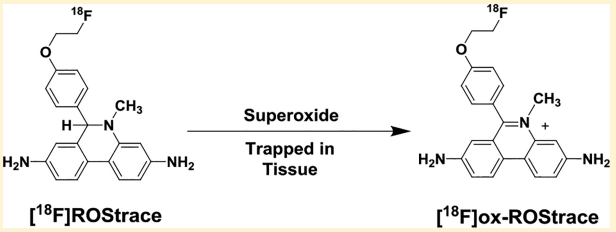

KEYWORDS: *Reactive oxygen species, Superoxide, Positron emission tomography, Neuroinflammation*

INTRODUCTION

The term reactive oxygen species (ROS) has been used to describe a class of highly reactive oxygen-containing molecules, including superoxide radical anion ($O_2^{\bullet-}$), hydrogen peroxide (H_2O_2), hydroxyl radical ($OH^{\bullet-}$), and hypochlorous acid (HOCl).[1−3] While ROS have a role in normal cellular processes, high levels of ROS can lead to oxidative stress and protein, lipid, and DNA damage. Consequently, ROS levels are tightly regulated in a cell through the activity of the enzymes, superoxide dismutase (SOD1−SOD3), catalase, and NADH peroxidase.[1,3] An imbalance between the rate of formation of ROS and the regulatory mechanisms resulting elevated ROS leads to a condition called oxidative stress.[4] Oxidative stress has been implicated in the pathogenesis of cardiovascular and neurodegenerative diseases and cancer.[1]

One major source of ROS is oxidative phosphorylation in the mitochondria, and mitochondrial dysfunction involving reduced Complex I activity is considered to be one of the main sources of elevated ROS levels in Parkinson's disease (PD).[2,3] Another main source of ROS are the nicotinamide adenine dinucleotide phosphate (NADPH) oxidases (NOX1−NOX5, DUOX1, and DUOX2), which make up a family of enzymes that transfer electrons from the reduced form of NADPH to molecular oxygen.[3,5] The NADPH oxidases have a widespread distribution throughout the body and are thought to play a key role in host defense, cellular signaling, stress response, and tissue homeostasis. Within the central nervous system (CNS), NOX1 and NOX4 are expressed in low levels in neurons, astrocytes, and microglial cells, whereas NOX2 is expressed in high levels in microglial cells. NOX2 is thought to be latent under normal conditions; upon microglial activation, NOX2 becomes activated through the formation of a multimeric protein complex leading to NOX2-derived superoxide formation.[5] This activation process is thought to play a key role in mediating proinflammatory, M1-polarized microglia in neuroinflammation, and increases in the levels of NOX2 and other markers of oxidative stress have been reported in post-mortem samples of Alzheimer's disease (AD) brain and in transgenic mouse models of AD.[4,6] Similar results have been reported in the substantia nigra of PD brain samples and in the 1-methyl-4-phenyl-1,2,3,6-tetrahydropyridine (MPTP) model of PD. In addition, the spinal cords of patients with amyotropic lateral sclerosis (ALS) have been reported to have increased levels of NOX2 expression and other measures of oxidative stress such as the elevation of the levels of COX-2 and other cytokines.[7] These results indicate that the proinflammatory form of neuroinflammation leading to the elevation of the levels of superoxide and ROS represents a common pathway in neurodegenerative disorders.

Received: October 9, 2017
Accepted: November 3, 2017
Published: November 3, 2017

DOI: 10.1021/acschemneuro.7b00385
ACS Chem. Neurosci. 2018, 9, 578−586

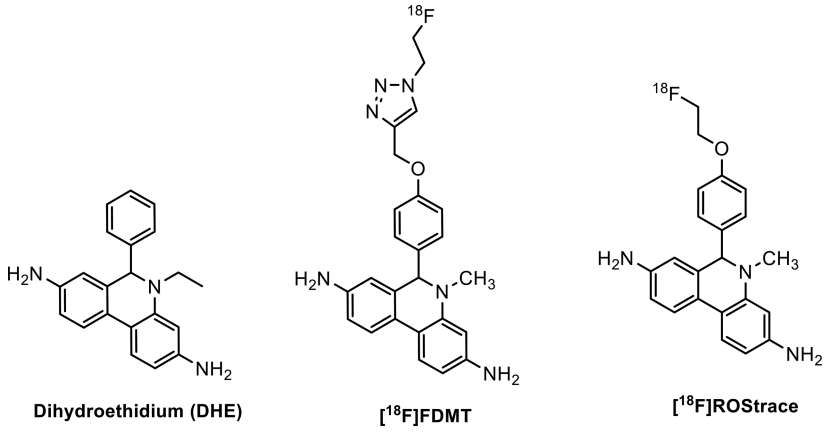

Figure 1. Structures of dihydroethidium, [^{18}F]FDMT, and [^{18}F]ROStrace.

Scheme 1

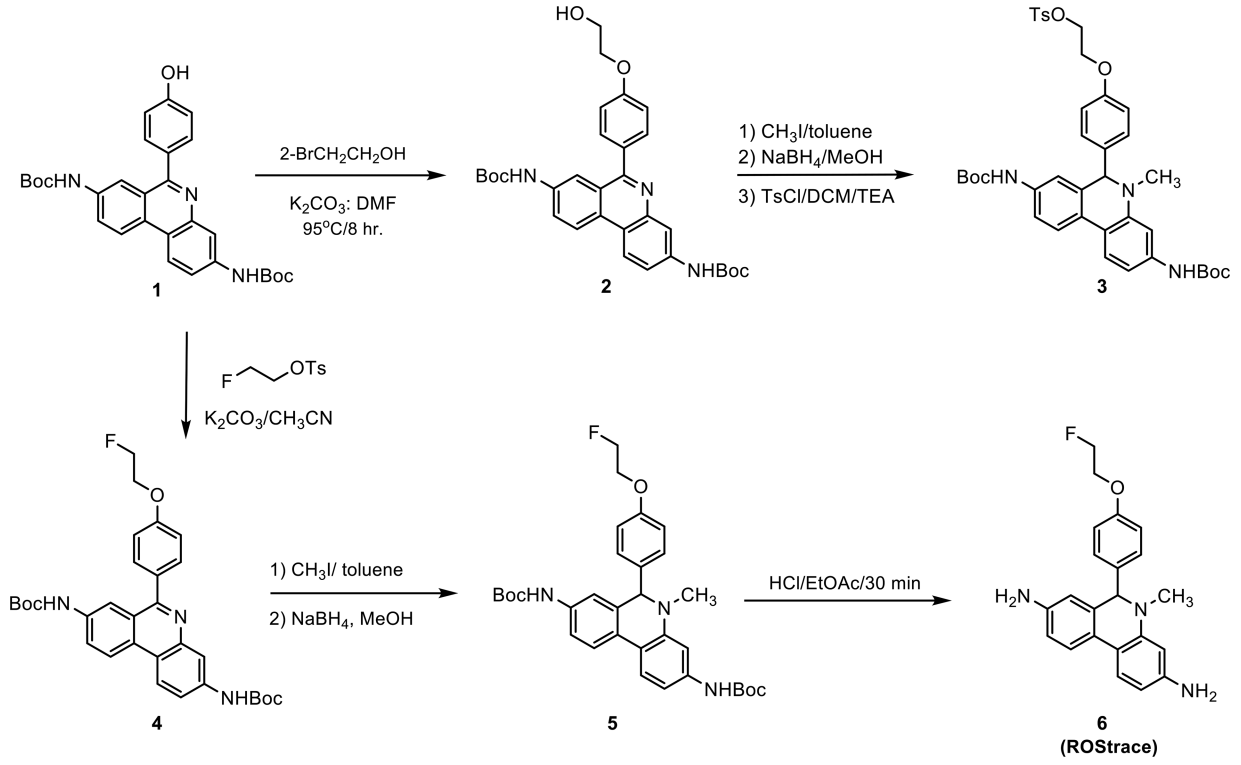

On the basis of the discussion given above, an imaging probe capable of measuring levels of superoxide in brain would be a valuable tool for measuring the proinflammatory, M1-polarized form of neuroinflammation. Furthermore, because neuroinflammation is thought to represent a hallmark in the pathophysiology of a number of neurodegenerative diseases,[7] a PET radiotracer for measuring superoxide levels in the CNS could provide insight into the relationship between the formation of ROS and other pathological features associated with neurodegeneration (e.g., Aβ and tau formation in AD).[8]

The fluorescent probe dihydroethidium (DHE) has been used to measure superoxide levels in cells and tissues using microscopy and optical imaging techniques.[9−11] Our group has previously reported the synthesis of an ^{18}F-labeled analogue of DHE, [^{18}F]FDMT, and its evaluation in an animal model of adriamycin-induced cardiotoxicity (Figure 1).[12] The results of this study were significant because they revealed for the first time the ability to image ROS in a living organism using positron emission tomography (PET). While this tracer was able to image ROS levels in peripheral organs in vivo, it did not cross the blood−brain barrier (BBB) to allow imaging of elevated superoxide levels associated with proinflammatory microglia activation. In the study presented here, we report the in vivo evaluation of an ^{18}F-labeled analogue of DHE, [^{18}F]ROStrace (Figure 1), which is capable of crossing the BBB. We also describe the series of in vivo validation studies confirming the ability of [^{18}F]ROStrace to image superoxide levels in a murine model of neuroinflammation.

RESULTS

Chemistry and Reactivity with Reactive Oxygen Species. The synthesis of ROStrace and its precursor for radiolabeling is shown in Scheme 1. The hydroxyethyl was introduced to the known hydroxy compound di-*tert*-butyl [6-

DOI: 10.1021/acschemneuro.7b00385
ACS Chem. Neurosci. 2018, 9, 578−586

(4-hydroxyphenyl)phenanthridine-3,8-diyl]dicarbamate[12] to form compound **2**, which was methylated with iodomethane, reduced with sodium borohydride, and then carefully tosylated to give precursor compound **3**. The standard compound, ROStrace (**6**), was synthesized (Scheme 1) using a similar procedure. Once the compounds were reduced, they were very labile especially in solution. All the following procedures were performed in a rapid manner at a low temperature.

The reactivity of DHE and ROStrace for superoxide, hydrogen peroxide, and hydroxyl radical was measured using an in vitro assay as previously reported.[12] Two different methods were used to generate superoxide, xanthine oxidase metabolism of hypoxanthine or thermal decomposition of 3-morpholinosyndnomine (SIN-1) in the presence of 2-(4-carboxyphenyl)-4,4,5,5-tetramethyl-imidazoline-1-oxyl-3-oxide (CPTIO). In the both systems, oxidation of ROStrace was completely prevented by the addition of superoxide dismutase (SOD) (Figure 2). ROStrace was also exposed to hydrogen peroxide alone or in the presence of horseradish peroxidase (HRP) to generate hydroxyl free radical. The fluorescence intensity results indicate that ROStrace has little reactivity with hydrogen peroxide or hydroxyl radical (Figure 2). These data suggest that ROStrace has good selectivity for superoxide. Because its chemical reactivity is similar to that of DHE, which is selectively oxidized to ethidium by superoxide radical (Figure 2), we believe ROStrace will behave like DHE in vivo and measure brain levels of superoxide radical.[13]

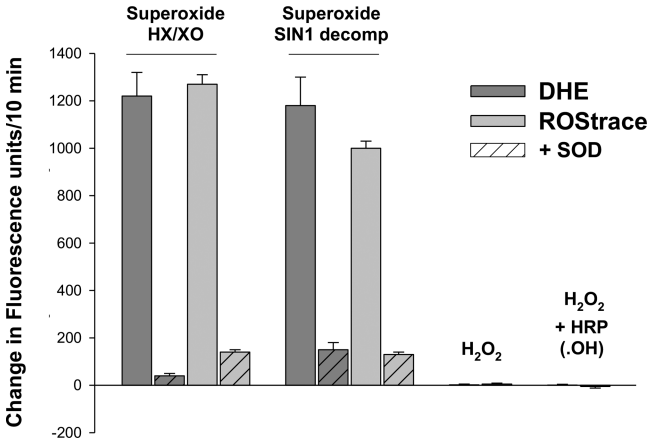

Figure 2. DHE and ROStrace are selectively oxidized by superoxide, but not by H_2O_2 or hydroxyl radical. ROStrace was exposed to superoxide (generated by two methods, xanthine oxidase metabolism of hypoxanthine and thermal decomposition of SIN-1 in the presence of CPTIO), hydrogen peroxide alone, or horseradish peroxidase (HRP) to generate hydroxyl free radical. Oxidation of ROStrace was prevented by the addition of superoxide dismutase (SOD).

Radiochemistry. [^{18}F]ROStrace was synthesized (Scheme 2) in an 8−12% radiochemical yield starting from [^{18}F]fluoride ion, with a molar activity of >74 GBq/μmol. To confirm the mechanism of uptake of radioactivity in the LPS-treated mice, [^{18}F]*ox*-ROStrace was also synthesized. This was accomplished by the quantitative conversion of [^{18}F]ROStrace to [^{18}F]*ox*-ROStrace by treatment with cupric sulfate (Scheme 2).

In Vivo Evaluation. The in vivo evaluation of [^{18}F]-ROStrace was performed using an LPS-treated mouse model of neuroinflammation. MicroPET imaging studies were conducted in both control (N = 15) and LPS-treated (N = 16) animals. The sagittal images revealed a much higher rate of brain uptake of [^{18}F]ROStrace in the LPS-treated animals than in the control group (Figure 3a). Time−activity curves from the control mice demonstrated that [^{18}F]ROStrace has a high initial rate of brain uptake, peaking within the first minute, followed by a rapid washout. In LPS-treated animals, activity continued to increase in the brain, peaking around 3 min post-injection (Figure 3b). Levels of brain activity in both control and LPS-treated mice stabilized after ∼20 min. However, the extent of retention of radioactivity in brain was higher in the LPS-treated mice.

The initial analysis of the group data involved a comparison of the average %ID/cm^3 values from 40 to 60 min post-injection of the radiotracer for the control versus LPS-treated animals. This time interval was chosen because it represents a plateau phase in the time−activity curves. A graph of the average %ID/cm^3 for the two groups (Figure 3c) revealed a statistically significant difference between the control and LPS-treated animals (P < 0.0001) even though there was some overlap between individual subjects in the LPS-treated group and the control group. When the LPS-treated mice were grouped as a whole and compared to the control group, a 156% increase in the rate of brain uptake was observed.

It was also observed that not all animals responded to the LPS treatment in the same manner. That is, some animals displayed symptoms more severe than the symptoms of others, while others appeared to be unaffected by the dose of LPS. To characterize the animals to the degree of "sickness" following the LPS treatment, a scoring mechanism based on criteria outlined by Carstens and Moberg[14] for recognizing pain and distress in laboratory animals was used. Using this method, animals were assigned a condition score based on visual observation of signs of distress, including hunched posture, decreased motion, piloerection, lack of grooming, and discharge from the eyes. The animals were then grouped into three levels

Scheme 2

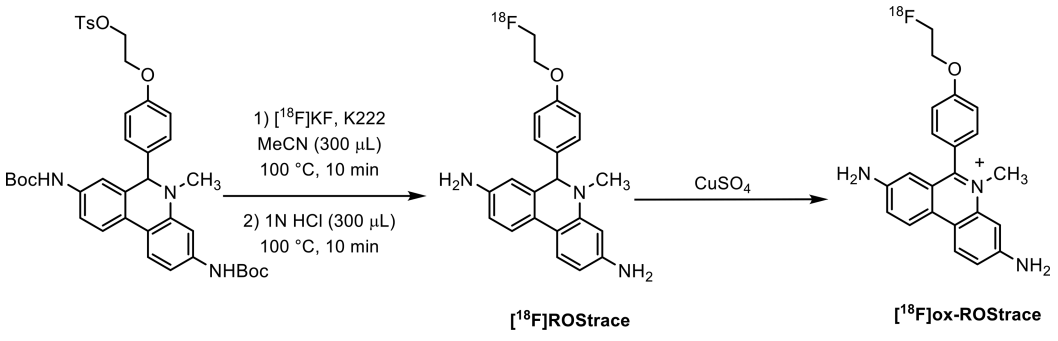

DOI: 10.1021/acschemneuro.7b00385
ACS Chem. Neurosci. 2018, 9, 578−586

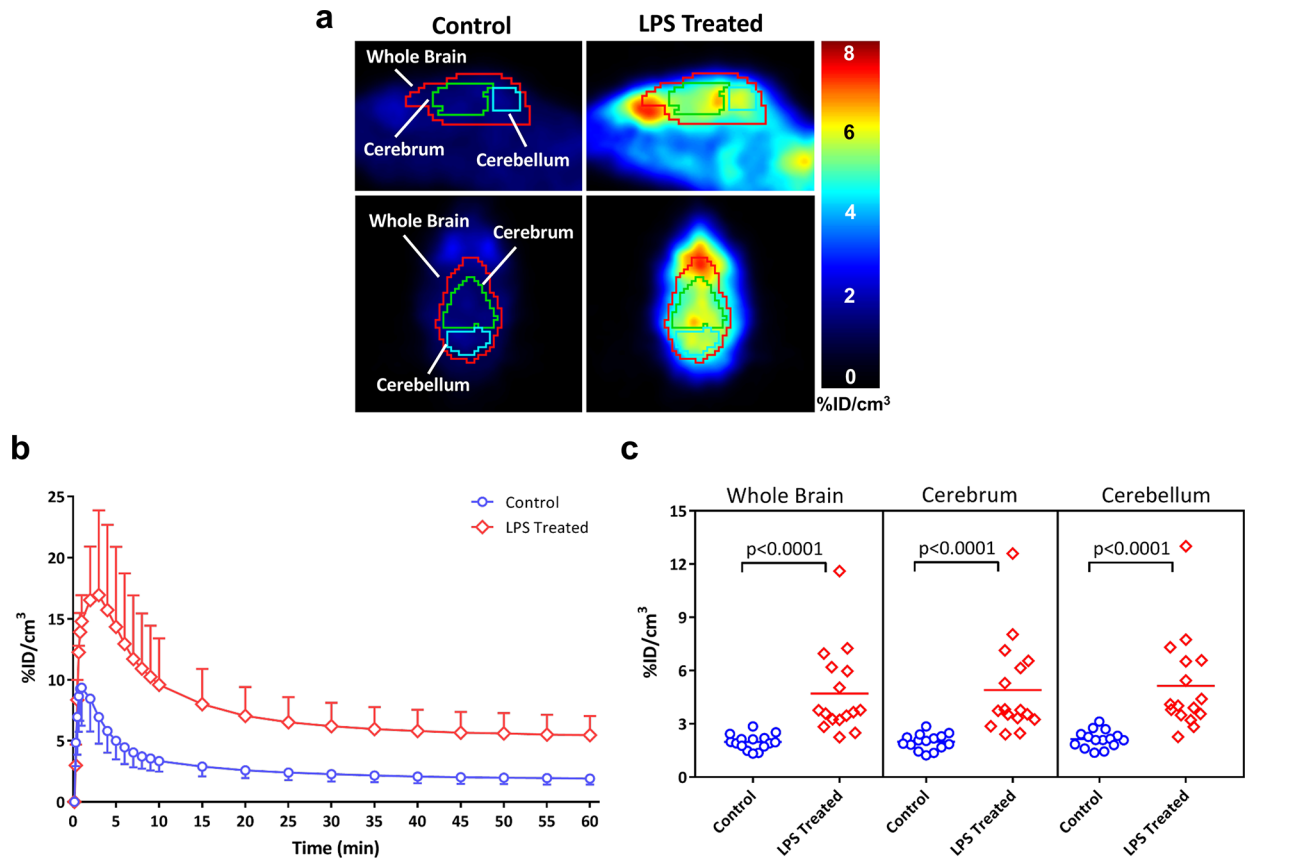

Figure 3. [^{18}F]ROStrace microPET imaging of control and LPS-treated mice. (a) Representative control and LPS-treated mouse images 40−60 min post-[^{18}F]ROStrace injection. (b) Time−activity curves demonstrate the high initial rate of brain uptake followed by a plateau after 40 min. %ID/cm^3 values were obtained from 40−60 min summed images (c) to show differential uptake in control vs LPS-treated mice.

of sickness. Level 1 animals displayed mild symptoms and appeared to be fairly normal. Level 2 animals displayed a moderate response, including some of the stated symptoms. Level 3 animals displayed practically all the symptoms more severely. The results of this analysis are shown in Figure 4. Animals with a condition score of 2 or 3 had a rate of uptake of [^{18}F]ROStrace significantly higher than those of the control group and level 1 animals. These data indicate that the difference in response to LPS as measured via the observational studies is predictive of the relative amount of neuroinflammation in the CNS.

To further confirm the mechanism of retention of [^{18}F]-ROStrace in the CNS, radiometabolite analysis of homogenates from brains obtained after completion of the microPET imaging studies was conducted. The results of the HPLC studies indicated that the activity in brain was primarily the oxidized species, [^{18}F]*ox*-ROStrace, while a much smaller amount of the parent compound was detected (68% vs 10%) 2 h after an intravenous injection of [^{18}F]ROStrace. Blood levels of the oxidized species are much lower (27%) at the same time point, suggesting that [^{18}F]*ox*-ROStrace is not entering the brain from the circulation (Table 1).

We believe the neutral species, [^{18}F]ROStrace, enters the brain where it is trapped upon oxidation to [^{18}F]*ox*-ROStrace by superoxide. To demonstrate that the higher level of retention of [^{18}F]ROStrace in LPS-treated mice is due to oxidation by LPS-induced ROS in the brain, and that the peripherally oxidized species, [^{18}F]*ox*-ROStrace, cannot enter the brain, mice were imaged after an injection of [^{18}F]*ox*-ROStrace. [^{18}F]*ox*-ROStrace showed no brain uptake in the untreated mice (Figure 5). These data demonstrate that the neutral species, [^{18}F]ROStrace, crosses the BBB and is oxidized to [^{18}F]*ox*-ROStrace after entering the brain. LPS treatment is known to cause some disruption of the BBB, and our LPS-treated mice displayed a small amount of brain uptake when they were imaged with [^{18}F]*ox*-ROStrace 24 h post-LPS treatment. The same imaging procedure performed 1 week after LPS treatment resulted in no uptake. These data confirm the trapping mechanism of [^{18}F]ROStrace in the brain is due to oxidation by superoxide to [^{18}F]*ox*-ROStrace (Figure 5).

Ex vivo autoradiography studies were conducted on brain sections harvested after completion of the PET imaging studies. In these studies, animals were treated with DHE (15 mg/kg, intravenous) 30 min prior to being sacrificed so that a comparison can be made between the distribution of the radiotracer, which is primarily [^{18}F]*ox*-ROStrace, and the fluorescent signal from oxidized DHE (i.e., ethidium/2-OH-ethidium). The results of this study indicate a similar pattern of distribution between the radiotracer and oxidized DHE fluorescence (Figure 6). We also obtained fluorescence images in mice 30 min after injection of cold ROStrace (14 mg/kg, intravenous). As expected, this also provided a similar pattern of distribution in the brain. These results further support the mechanism of uptake and trapping of [^{18}F]ROStrace in the CNS under high-ROS conditions.

DOI: 10.1021/acschemneuro.7b00385
ACS Chem. Neurosci. 2018, 9, 578−586

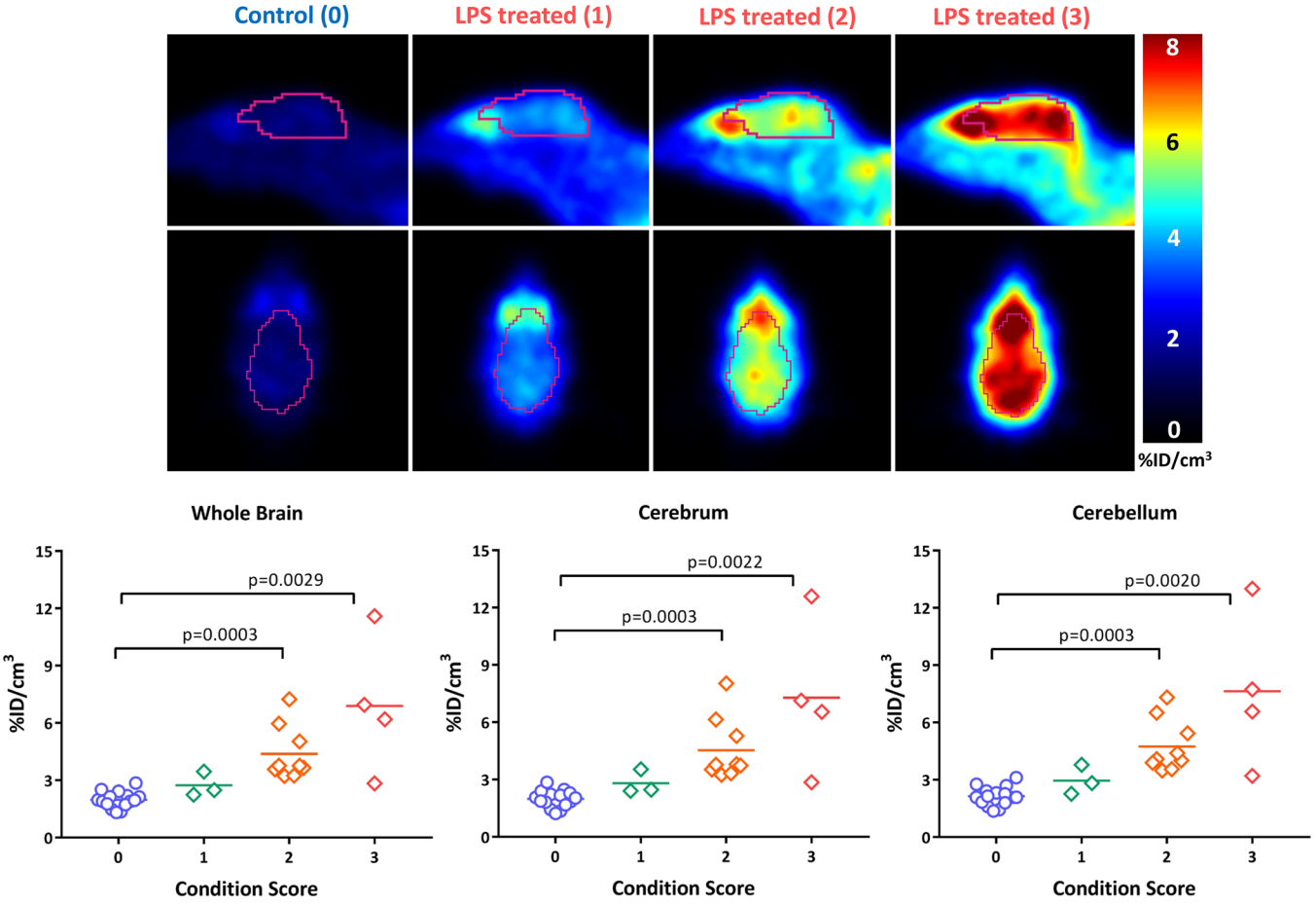

Figure 4. Stratification of LPS-treated mice based on condition score suggests that a higher rate of brain uptake of [^{18}F]ROStrace correlates with greater severity of symptoms from LPS treatment.

Table 1. Metabolite Analysis of Blood and Brain Homogenates 2 h Post-[^{18}F]ROStrace Injection

	polar	[^{18}F]ROStrace	[^{18}F]*ox*-ROStrace
brain	7.0 ± 1.9	10.0 ± 2.5	68.3 ± 2.2
blood	23.8 ± 8.2	31.8 ± 7.3	27.0 ± 2.3

DISCUSSION

The goal of this study was to develop a PET radiotracer for imaging superoxide levels in the CNS that are produced during the proinflammatory, M1-polarized form of neuroinflammation that is thought to be a hallmark feature of neurodegeneration.[7,8,15] Our group previously reported an ^{18}F-labeled analogue of the fluorescent probe DHE and demonstrated that it was capable of imaging superoxide that is produced in myocardial tissues in an animal model of adriamycin-induced cardiotoxicity.[12] Although this probe is capable of imaging superoxide in peripheral organs, its inability to cross the BBB prevented its use as a means of imaging superoxide produced under conditions of neuroinflammation and mitochondrial dysfunction, which are thought to occur in most neurodegenerative disorders.

In the time interval between our initial publication and this study, a number of ROS-based radiotracers have been reported in the literature. These include (1) [^{18}F]PC-FLT, which measures extracellular and intracellular levels of H_2O_2,[16] (2) [^{11}C]vitamin C, which measures extracellular levels of H_2O_2,[17] (3) the hydrocyanine dye derivative, [^{18}F]ROS1, which measures superoxide and hydroxyl radicals,[18] (4) [^{18}F]-5-fluoroaminosuberic acid, which provides an indirect measure of intracellular levels of ROS by imaging the increase in the level of expression of the cystine transporter (system x_c-),[19] and (5) [^{11}C]DHQ1, a dihydroisoquinoline analogue that can be used to measure intracellular levels of superoxide.[20] [^{11}C]DHQ1 is capable of crossing the BBB and has potential for imaging increased ROS levels in the CNS as a consequence of neuroinflammation.[20] A number of radiolabeled analogues of dihydro-methidium (also known as hydromethidine) have been synthesized and evaluated in vitro and in vivo, including [^{3}H]hydromethidine and [^{11}C]hydromethidine.[21,22] [^{3}H]-Hydromethidine is oxidized by superoxide and hydroxyl radicals and has been evaluated in animal models of stroke and cisplatin-induced nephrotoxicity.[23,24] A recent paper on the radiosynthesis and preliminary in vivo evaluation of [^{11}C]-methidium has also been reported.[22] It should also be noted that our group reported the in vitro properties of methidium toward various forms of ROS in the patent literature (U.S. Patent 9,035,057) but did not pursue radiolabeling of this compound because of our interest in developing an ^{18}F-labeled radiotracer for imaging ROS.

In the study presented here, we report the synthesis, in vitro characterization, and in vivo evaluation of [^{18}F]ROStrace in an LPS treatment model of neuroinflammation. In vitro studies indicate that it is oxidized to the charged species, [^{18}F]*ox*-ROStrace, by superoxide because it has low reactivity for hydrogen peroxide and hydroxyl radical (Figure 2). Our in vivo

DOI: 10.1021/acschemneuro.7b00385
ACS Chem. Neurosci. 2018, 9, 578−586

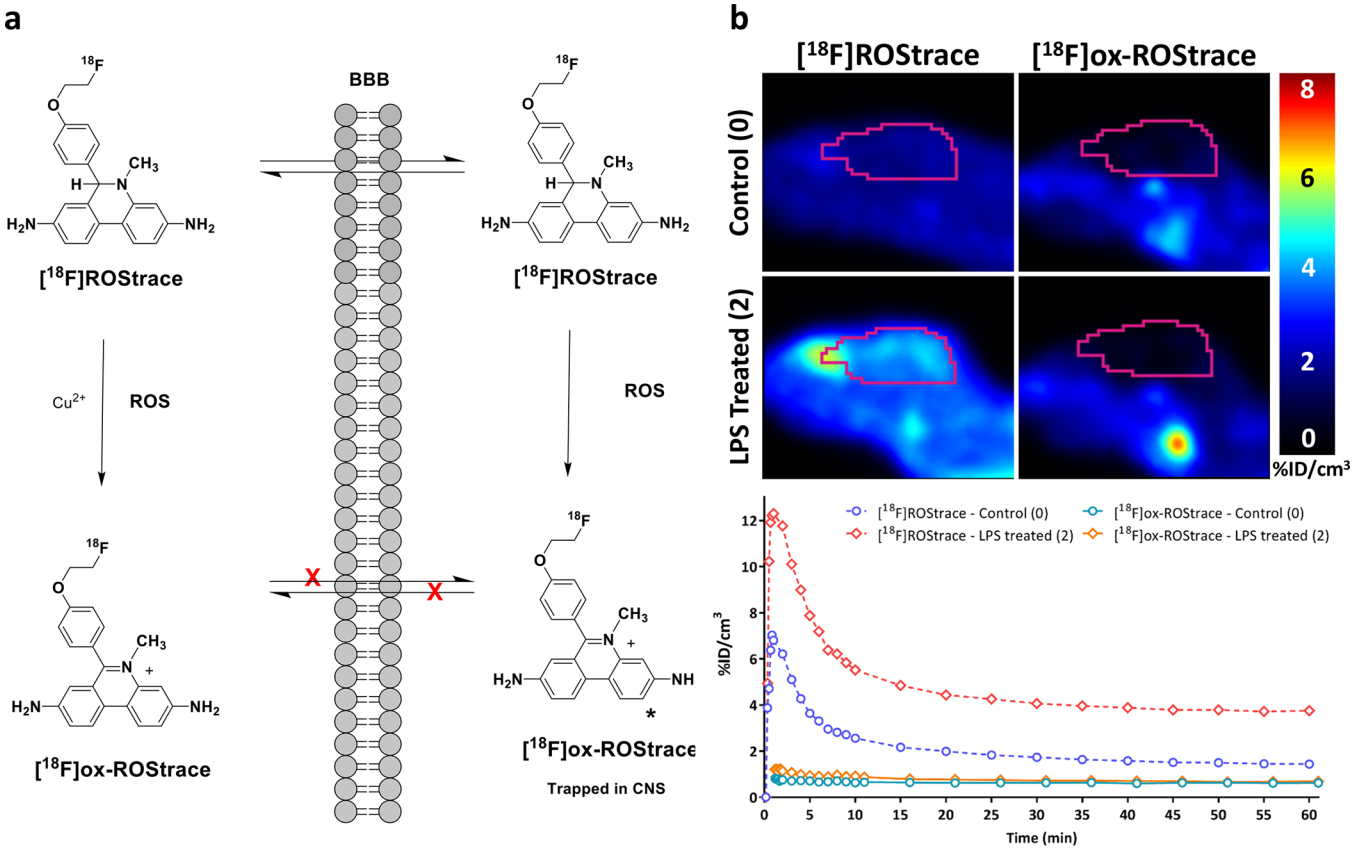

Figure 5. Demonstration that [^{18}F]*ox*-ROStrace does not cross the BBB. (a) Mechanism of brain uptake and retention of [^{18}F]ROStrace. (b) MicroPET images and time−activity curves comparing brain uptake of [^{18}F]ROStrace and [^{18}F]*ox*-ROStrace.

studies included not only the uptake of the parent radiotracer, [^{18}F]ROStrace, in LPS-treated versus control mice but also a detailed metabolite analysis study confirming the mechanism of uptake and trapping of the radiotracer in the CNS. This trapping mechanism was also confirmed by the observation that the oxidized species, [^{18}F]*ox*-ROStrace, is not capable of crossing the BBB. The distribution of radioactivity in the LPS-treated animals also matched the distribution of the fluorescence signal from treatment of the animals post-PET with DHE, which further supports the mechanism of trapping of the radiotracer in the CNS. Our results revealed that the relative uptake and retention of [^{18}F]ROStrace correlated with the level of sickness induced by LPS, which suggests that this radiotracer is capable of measuring different levels of neuroinflammation in rodent models of neurodegeneration. Taken collectively, our data demonstrate that [^{18}F]ROStrace is the first ^{18}F-labeled radiotracer capable of measuring elevated levels of superoxide that occur during the "neurotoxic" or proinflammatory form of neuroinflammation.

CONCLUSION

[^{18}F]ROStrace is a promising PET radiotracer for imaging elevated superoxide levels in the CNS under conditions of neuroinflammation. We are currently using this radiotracer in a panel of transgenic mouse models of AD, PD, and other neurodegenerative disorders.

METHODS

General. All chemicals were purchased from commercial sources and were used without further purification. Nuclear magnetic resonance (NMR) spectra were recorded on a Bruker DMX 500 MHz spectrometer. Using the ESI technique on a model 2695 Alliance LCMS instrument, mass spectroscopy data were acquired and compound purity analysis was performed. Target compounds were purified on a Biotage Isolera One instrument with a dual-wavelength ultraviolet−visible detector. Chemical shifts (δ) in the ^{1}H NMR spectra were referenced by assigning the residual solvent peaks. Elemental analyses were performed by Atlantic Microlabs, Inc. (Atlanta, GA) and were within ±0.4% unless otherwise noted. The reactivity for ROS was measured using the published method.[12]

*Di-tert-butyl {6-[4-(2-Hydroxyethoxy)phenyl]phenanthridine-3,8-diyl}dicarbamate (**2**).* Di-*tert*-butyl [6-(4-hydroxyphenyl)-phenanthridine-3,8-diyl]dicarbamate[12] (501 mg, 1 mmol), 2-bromoethanol (400 mg, 3.22 mmol), potassium carbonate (690 mg, 5 mmol), and dimethylformamide (DMF) (6 mL) were placed in a sealed vial and heated to 95 °C overnight. The mixture was diluted with water (50 mL) and extracted with ethyl acetate. The organic layer was washed with H_2O, aqueous $NaHCO_3$, and brine (twice each) and dried with Na_2SO_4. After filtration, the filtrate was condensed and the residue was applied to FC [dichloromethane/ethyl acetate (0−40%)] yielding compound **1** (340 mg, 62%) and the recovered starting material: ^{1}H NMR (500 MHz, DMSO-d_6) δ 1.45 (s, 9H), 1.51 (s, 3H), 3.79 (dt, J = 5.1, 4.9 Hz, 2H), 4.11 (t, J = 4.9 Hz, 2H), 4.92 (t, J = 5.5 Hz, 1H), 7.13 (d, J = 8.6 Hz, 2H), 7.65 (d, J = 8.6 Hz, 2H), 7.77 (dd, J = 8.9, 2.0 Hz, 1H), 8.00 (d, J = 8.6 Hz, 1H), 8.17 (s, 1H), 8.25 (s, 1H), 8.56 (d, J = 9.1 Hz, 1H), 8.67 (d, J = 9.2 Hz, 1H), 9.67 (s, 1H), 9.69 (s, 1H); ^{13}C NMR (500 MHz, DMSO-d_6) δ 28.06, 28.12, 59.59, 69.69, 79.34, 114.11, 115.13, 116.29, 118.14, 118.69, 122.46, 122.67, 122.93, 124.38, 128.10, 131.04, 131.86, 138.08, 139.45, 143.31, 152.76, 152.78, 159.06, 159.83; HRMS calcd for $C_{31}H_{36}N_3O_6^+$ [M + H]$^+$ 546.2599, found 546.2626.

*2-(4-{3,8-Bis[(tert-butoxycarbonyl)amino]-5-methyl-5,6-dihydrophenanthridin-6-yl}phenoxy)ethyl 4-Methylbenzenesulfonate (**3**).* Compound **2** (120 mg, 0.22 mmol) was suspended in a mixture of

DOI: 10.1021/acschemneuro.7b00385
ACS Chem. Neurosci. 2018, 9, 578−586

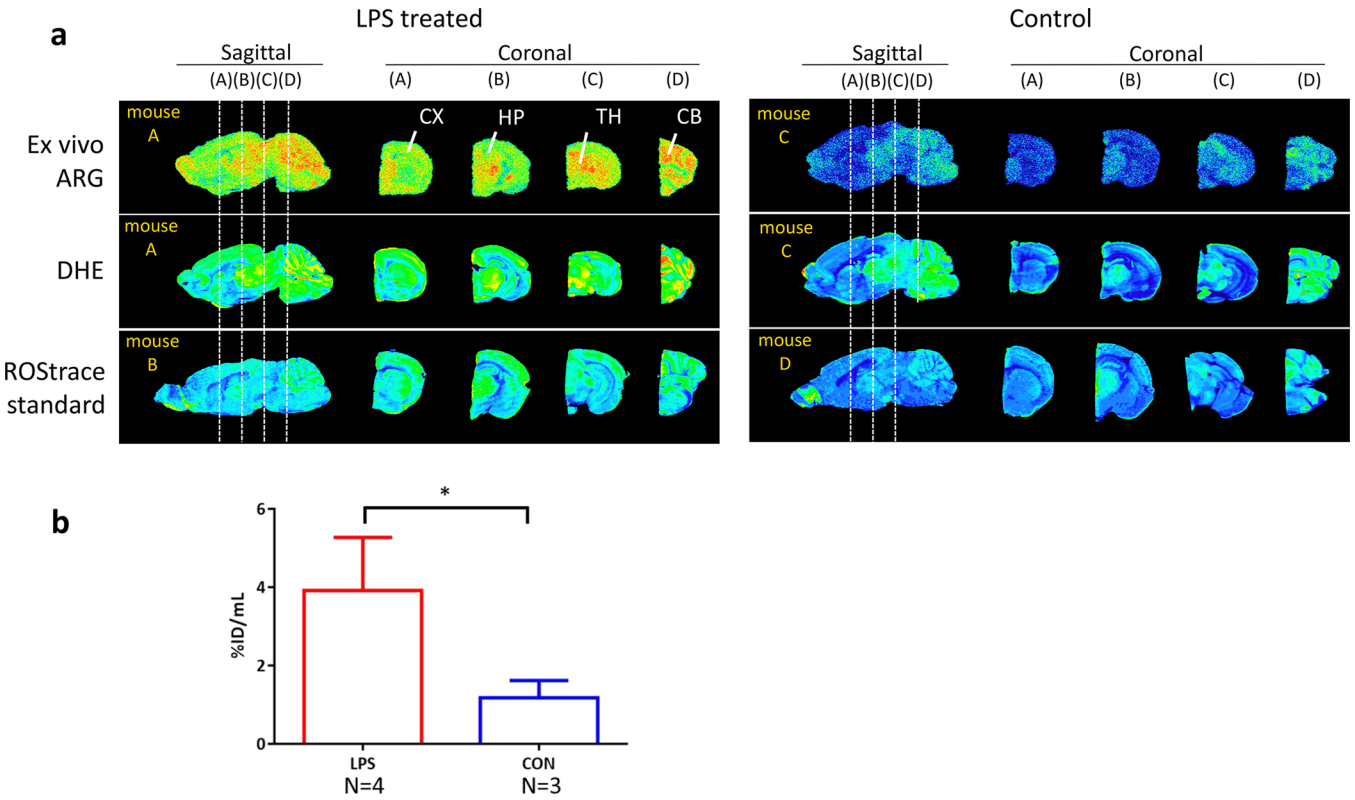

Figure 6. Distribution pattern of [^{18}F]ROStrace that is comparable with the fluorescent signal from DHE or ROStrace. (a) Direct comparison of ex vivo [^{18}F]ROStrace autoradiography with DHE fluorescence in the same brain section. The distribution is also comparable with ROStrace fluorescence performed in separate animals. Abbreviations: ARG, autoradiography; DHE, dihydroethidium; CX, cortex; HP, hippocampus; CB, cerebellum. (b) LPS-treated mice showed a significantly higher rate of [^{18}F]ROStrace uptake (*P < 0.0001) compared with that of nontreated animals by ex vivo autoradiography.

toluene (9 mL) and iodomethane (1 mL) and stirred at 70 °C overnight. The mixture was condensed under vacuum, and the residue was dissolved in 5 mL of methanol. The mixture was cooled with an ice bath, and an excess of $NaBH_4$ (~30 mg) was added. The mixture was stirred at 0 °C for 10 min and condensed under vacuum below 10 °C. The residue was applied to a pre-equilibrated column of silica and eluted with dichloromethane/ethyl acetate (0−40%). The combined fractions were condensed below 10 °C, yielding the methylated compound (67 mg, 54%) as a slightly brown solid. This compound (67 mg, 0.12 mmol) was then dissolved in dichloromethane (3 mL) at 0 °C, and *p*-toluenesulfonyl chloride (84 mg, 0.44 mmol) and trimethylamine (120 mg, 1.2 mmol) were added. The reaction mixture was stirred at 0 °C for 2 h, applied to a pre-equilibrated column of silica gel, and eluted with dichloromethane/ethyl acetate (0−15%). The proper fractions were combined and condensed below 10 °C, yielding the title compound as a slightly red solid (65 mg, 76%): ^{1}H NMR (500 MHz, $CDCl_3$) δ 1.48 (s, 9H), 1.50 (s, 3H), 2.40 (s, 3H), 2.83 (s, 3H), 4.01 (t, J = 4.8 Hz, 2H), 4.28 (t, J = 4.8 Hz, 2H), 4.92 (t, J = 5.5 Hz, 1H), 5.22 (s, 1H), 6.47 (s, 2H), 6.54 (d, J = 8.7 Hz, 2H), 6.72 (s, 2H), 6.98 (d, J = 8.7 Hz, 2H), 7.15 (s, 1H), 7.17 (s, 1H), 7.28 (d, J = 8.1 Hz, 2H), 7.57 (d, J = 8.8 Hz, 1H), 7.64 (d, J = 9.0 Hz, 1H), 7.76 (d, J = 8.3 Hz, 2H); ^{13}C NMR (500 MHz, $CDCl_3$) δ 21.56, 28.29, 28.33, 37.06, 65.29, 67.18, 68.04, 80.30, 80.45, 102.35, 107.54, 114.45, 116.34, 117.01, 117.86, 122.66, 123.03, 125.50, 127.92, 127.97, 128.10, 128.95, 129.77, 132.84, 134.35, 135.72, 137.01, 139.14, 144.86, 152.52, 157.38; HRMS calcd for $C_{39}H_{46}N_3O_8S^+$ [M + H]$^+$ 716.3000, found 716.3016.

*Di-tert-butyl {6-[4-(2-Fluoroethoxy)phenyl]phenanthridine-3,8-diyl}dicarbamate (**4**).* Di-*tert*-butyl [6-(4-hydroxyphenyl)-phenanthridine-3,8-diyl]dicarbamate[12] (1.04 g, 2.07 mol) was dissolved in MeCN, and 2-fluoroethyl tosylate (902 mg, 4.14 mmol) and K_2CO_3 (855 mg, 6.22 mmol) were added. The reaction mixture was heated to 80 °C and allowed to stir overnight. The reaction mixture was filtered and concentrated to give a residue that was purified by FC [DCM/ethyl acetate (0−50%)] to afford the desired compound as off-white foam (800 mg, 70%): ^{1}H NMR (500 MHz, DMSO-d_6) δ 1.45 (s, 9H), 1.51 (s, 9H), 4.36 (dt, J = 30.1, 3.8 Hz, 2H), 4.81 (dt, J = 47.9, 3.8 Hz, 2H), 7.16 (d, J = 8.7 Hz, 2H), 7.66 (d, J = 8.7 Hz, 2H), 7.77 (dd, J = 9.0, 2.2 Hz, 1H), 8.00 (d, J = 8.7 Hz, 1H), 8.56 (d, J = 9.1 Hz, 1H), 8.67 (d, J = 9.1 Hz, 1H), 9.67 (s, 1H), 9.69 (s, 1H); ^{13}C NMR (500 MHz, DMSO-d_6) δ 28.08, 28.14, 67.15, 67.31, 79.38, 81.52, 82.85, 114.18, 115.06, 116.27, 118.18, 118.73, 122.54, 122.69, 123.01, 124.39, 128.12, 131.14, 132.32, 138.13, 139.49, 143.32, 152.78, 152.81, 158.52, 159.79; HRMS calcd for $C_{31}H_{35}FN_3O_5$ [M + H]$^+$ 548.2555, found 548.2545.

*Di-tert-butyl {6-[4-(2-Fluoroethoxy)phenyl]-5-methyl-5,6-dihydrophenanthridine-3,8-diyl}dicarbamate (**5**).* A screw-cap vial containing a solution of di-*tert*-butyl {6-[4-(2-fluoroethoxy)phenyl]-phenanthridine-3,8-diyl}dicarbamate (**4**, 45 mg, 0.082 mmol) in toluene (1.5 mL) was treated with 0.50 mL of iodomethane. The vial was briefly purged with nitrogen, sealed, and heated to 95 °C for 6 h. The reaction mixture was then moved to a 75 °C bath and allowed to stir overnight. The reaction mixture was condensed and taken up in EtOH (2 mL). The solution was treated with excess $NaBH_4$ (7 mg) and concentrated to give a residue that was purified by FC [DCM/ethyl acetate (0−30%)] to give the desired product as a colorless solid (35 mg, 75%): ^{1}H NMR (500 MHz, $CDCl_3$) δ 1.48 (s, 9H), 1.50 (s, 9H), 2.85 (s, 3H), 4.08 (dt, J = 30.1, 4.2 Hz, 2H), 4.67 (dt, J = 47.4, 4.2 Hz, 2H), 5.24 (s, 1H), 6.45 (9s, 1H), 6.46 (s, 1H), 6.69−6.73 (m, 4H), 7.03 (d, J = 8.7 Hz, 2H), 7.58 (d, J = 8.1 Hz, 1H), 7.66 (d, J = 8.7 Hz, 1H); ^{13}C NMR (500 MHz, $CDCl_3$) δ 28.30, 28.34, 37.08, 66.86, 67.03, 67.20, 80.42, 80.73, 81.16, 82.52, 102.36, 107.48, 114.48, 117.04, 117.84, 122.69, 123.05, 125.52, 128.06, 134.15, 135.78, 136.99, 139.11, 144.87, 152.56, 157.80; HRMS calcd for $C_{32}H_{39}FN_3O_5$ [M + H]$^+$ 564.2868, found 564.2880.

DOI: 10.1021/acschemneuro.7b00385
ACS Chem. Neurosci. 2018, 9, 578−586

*6-[4-(2-Fluoroethoxy)phenyl]-5-methyl-5,6-dihydrophenanthridine-3,8-diamine (**6**).* Di-*tert*-butyl {6-[4-(2-fluoroethoxy)phenyl]-5-methyl-5,6-dihydrophenanthridine-3,8-diyl}dicarbamate (**5**, 20 mg, 0.035 mmol) was dissolved in EtOAc (1.5 mL), and concentrated HCl (37%, 0.5 mL) was added. The reaction mixture was purged with nitrogen and left to stir at room temperature for 30 min. The reaction mixture was neutralized with 7 N NH_3 in methanol and concentrated under high vacuum to give a rose-colored solid. The solid was dissolved in DCM and applied to FC (ethyl acetate) to afford the title compound as a colorless solid (12 mg, 93%): ^{1}H NMR (500 MHz, $CDCl_3$) δ 2.80 (s, 3H), 4.10 (dt, J = 30.2, 4.2 Hz, 2H), 4.68 (dt, J = 47.4, 4.2 Hz, 2H), 5.13 (s, 1H), 5.92 (d, J = 2.2 Hz, 1H), 6.18 (dd, J = 8.1, 2.1 Hz, 1H), 6.34 (d, J = 2.4 Hz, 1H), 6.61 (dd, J = 8.4, 2.4 Hz, 1H), 6.72 (d, J = 8.7 Hz, 2H), 7.05 (d, J = 8.7 Hz, 2H), 7.45 (d, J = 8.2 Hz, 1H), 7.52 (d, J = 8.4 Hz, 1H); ^{13}C NMR (500 MHz, $CDCl_3$) δ 37.03, 66.87, 67.03, 67.43, 81.18, 82.54, 99.52, 104.81, 112.98, 114.27, 114.41, 115.09, 122.17, 122.69, 122.95, 128.09, 134.61, 135.60, 144.47, 144.85, 146.47, 157.70; HRMS calcd for $C_{22}H_{23}N_3OF$ $[M + H]^+$ 364.1820, found 364.1831.

Radiochemistry. The radiosynthesis of [^{18}F]ROStrace was accomplished on an All-in-One module (Trasis, Ans, Belgium) with full automation. Briefly, [^{18}F]fluoride (800 mCi) was produced by proton irradiation of enriched $H_2{}^{18}O$ via the reaction of ^{18}O (p, n) ^{18}F by the Cyclone cyclotron (IBA). The [^{18}F]fluoride in a $H_2{}^{18}O$ solution is delivered to the hotcell, trapped on a preactivated Sep-Pak Light QMA Carb cartridge (Waters), and eluted to the reaction vial with 1 mL of eluent containing 2 mg of potassium carbonate and 7 mg of Kryptofix in a mixture of 0.85 mL of acetonitrile and 0.15 mL of water. The residual water was evaporated azotropically with 1 mL of acetonitrile at 100 °C under a stream of nitrogen gas and vacuum. A solution of 4 mg of tosylate precursor in 0.6 mL of methyl sulfide (DMSO) was added to the reaction vial for a 10 min reaction, followed by a 10 min deprotection with 1.0 mL of 1 N HCl. The reaction mixture was cooled to 50 °C and neutralized with 0.8 mL of 1 N NaOH. The crude product was diluted with 5 mL of the mobile phase and passed through an Alumina N Light cartridge (Waters) and a 0.45 μm nylon filter to the HPLC loop for high-performance chromatography (HPLC). A Phenomenex Luna C18 (2) semi-preparative column (10 mm × 250 mm) with a mobile phase of acetonitrile, water, and TFA (15:85:0.1 by volume) was used for HPLC purification. At a flow rate of 5 mL/min, the product was eluted at 18 min and diluted with water to a volume of 21 mL. The intermediate (oxidized byproduct) was then eluted with 65% acetonitrile with water. The diluted product solution was passed through a Sep-Pak Plus C18 cartridge (Waters). The trapped product was rinsed with water to waste and then eluted with ethanol (0.6 mL, with 0.1% ascorbic acid) followed by 8 mL of normal saline to the final production vial through a 0.2 μm nylon filter. After being shaken well, the final product was ready for quality control (QC) and animal studies. The yield ranged from 8 to 12% (decay corrected to the start of synthesis) in an average time of 65 min from receipt of [^{18}F]fluoride in a $H_2{}^{18}O$ solution from the cyclotron.

For the oxidized analogue, [^{18}F]*ox*-ROStrace, [^{18}F]ROStrace was oxidized by adding 2 mL of a 25 mM cupric sulfate aqueous solution. HPLC purification utilized a Sunfire C18 column (Waters, 10 mm × 250 mm) with a mobile phase of 35% acetonitrile in a 20 mM ascorbic acid solution. The retention time is approximately 10 min with a flow rate of 5 mL/min. The enrichment and final formulation are the same as those used for [^{18}F]ROStrace.

Animal Models. All animal studies were performed under protocols approved by the University of Pennsylvania Institutional Animal Care and Use Committee. Balb/c mice (Charles River) were injected intraperitoneally with 5 mg of LPS/kg from *E. coli* 0111:B4 (Sigma-Aldrich) 24 h prior to imaging studies. Mice were maintained on 2% isoflurane anesthesia and placed on a warm pad for scanning. Animals were euthanized at the completion of the scanning procedure by cervical dislocation and the brain and blood extracted for HPLC analysis of the identity of the radioactive species present or autoradiography.

Assessment of the Condition. The effect of LPS treatment on the animals was evaluated by visual observation of indicators, including hunched posture, decreased motion, piloerection, lack of grooming, and discharge from the eyes. This method was developed by combining different animal condition scoring systems and adapting them for common symptoms of LPS treatment. Condition scores ranged from 0 (normal) to 4 (moribund) and were obtained by scoring each animal for the presence of each indicator and whether the symptom was mild or severe (0, 1, or 2). After all indicators were added together, the possible totals (0−10) were subdivided into the final condition scores, 0−4. No treated animals were scored 0 or 4 in this study. Animals consistently lost approximately 10% body weight at 24 h post-LPS treatment, even level 1 animals, so weight was measured but not included as a factor.

PET Imaging. Mouse imaging was performed on the Philips MOSAIC HP small animal PET scanner, developed in collaboration with Philips Medical Systems. Dynamic images were acquired up to 60 min, after an intravenous injection of 200−300 μCi of [^{18}F]ROStrace or [^{18}F]*ox*-ROStrace. The slice thickness was $^1/_2$ mm and the field of view 12.8 cm. Data reconstruction was performed using the 3D-RAMLA protocol with decay correction turned on and normalization set for efficiency. Time−activity curves were constructed by plotting the normalized percent injected dose per cubic centimeter (normalized %ID/cm^3) versus time for a region of interest encompassing the entire brain. When comparisons were made between control and LPS-treated animals, the average %ID/cm^3 tissue for the 40−60 min period post-injection of [^{18}F]ROStrace was used because this represents a plateau phase in the time−activity curves (i.e., Δ %ID/cm^3 = 0). Three different regions of interest (whole brain, cerebrum, and cerebellum) were used for the data analysis shown in Figures 3 and 4.

Ex Vivo Autoradiography. Immediately after being imaged, mice were injected intravenously with 15 mg of DHE/kg (Sigma-Aldrich), and brains were harvested 30 min later and sectioned on a cryostat microtome. Sections were exposed to phosphor plates to obtain autoradiographic [^{18}F]ROStrace and fluorescent DHE images (GE Typhoon).

Metabolite Analysis. Blood samples and brains were collected from mice immediately postscan, and an acetonitrile/PBS (1:1) mixture was added at twice the volume of each sample. The blood solution was vortexed, and brains were homogenized with a pellet pestle, followed by centrifugation at 3000*g* for 10 min. After the supernatant had been separated from the pellet, each portion was counted with a gamma counter (PerkinElmer Wizard 2480) to determine the extraction efficiency. Part of the supernatant (>200 μL) was diluted with the same volume of water and then filtered with a 0.45 μm nylon filter, and 200 μL of the filtered supernatant was injected into an analytical metabolite HPLC instrument (1200 series, Agilent Technologies) equipped with an Agilent SB-C18 column (5 μm, 25 cm × 4.6 mm) and a fraction collector (Waters). The gradient mobile phase consisted of acetonitrile and a 0.1% TFA solution, and the flow rate was 1 mL/min. A fraction was collected every 30 s and counted with the gamma counter or directly with the LabLogic Laura Posi-RAM radiodetector.

Statistical Analysis Methods. A nonparametric Mann−Whitney test was used to compare the normalized %ID/cm^3 difference between control and LPS-treated groups. A multiple-group comparison among control and each condition level group was calculated by the nonparametric Kruskal−Wallis test with Dunn's post hoc test. A P value of <0.05 was considered to be a statistically significant difference.

AUTHOR INFORMATION

Corresponding Author

*University of Pennsylvania, Chemistry Building, Room 283, 231 S. 34th St., Philadelphia, PA 19104. E-mail: rmach@mail.med.upenn.edu.

ORCID

Catherine Hou: 0000-0001-8905-8492

Robert H. Mach: 0000-0002-7645-2869

DOI: 10.1021/acschemneuro.7b00385
ACS Chem. Neurosci. 2018, 9, 578−586

Author Contributions

R.H.M., L.L.D., and M.A.M. conceived of the project. C.H. and R.H.M. managed the study. T.J.G., K.X., and W.C. conducted organic synthesis. S.L. and T.J.G. conducted radiochemistry. S.L. and H.L. performed analytical quality control. S.K.C. and L.L.D. conducted the in vitro ROS assay. C.H. prepared the animals and performed the imaging studies. C.-C.W. performed the autoradiography. C.-J.H. and R.K.D. processed images and performed the PET data analysis. C.H., C.-J.H., S.L., K.X., and R.H.M. wrote the manuscript.

Funding

This research was funded by a grant from the Michael J. Fox Foundation (R.H.M.) and National Institutes of Health Grant AG033679-05 (L.L.D.).

Notes

The authors declare the following competing financial interest(s): The radiotracer described in this work is covered under U.S. Patent 9,035,057 B2 (W.C., L.L.D., M.A.M., and R.H.M., inventors).

■ ACKNOWLEDGMENTS

The authors thank Eric Blankemeyer and the University of Pennsylvania Small Animal Imaging Facility for assistance with microPET imaging.

■ REFERENCES

(1) Krumova, K., and Cosa, G. (2016) Overview of Reactive Oxygen Species. In *Singlet Oxygen: Applications in Biosciences and Nanosciences*, Vol. *1*, Chapter 1, pp 1−21, The Royal Society of Chemistry, Cambridge, U.K.

(2) Patten, D. A., Germain, M., Kelly, M. A., and Slack, R. S. (2010) Reactive oxygen species: stuck in the middle of neurodegeneration. *J. Alzheimer's Dis. 20*, S357−367.

(3) Sies, H., Berndt, C., and Jones, D. P. (2017) Oxidative Stress. *Annu. Rev. Biochem. 86*, 715−748.

(4) Klein, J. A., and Ackerman, S. L. (2003) Oxidative stress, cell cycle, and neurodegeneration. *J. Clin. Invest. 111*, 785−793.

(5) Haslund-Vinding, J., McBean, G., Jaquet, V., and Vilhardt, F. (2017) NADPH oxidases in oxidant production by microglia: activating receptors, pharmacology and association with disease. *British journal of pharmacology 174*, 1733−1749.

(6) Ganguly, G., Chakrabarti, S., Chatterjee, U., and Saso, L. (2017) Proteinopathy, oxidative stress and mitochondrial dysfunction: cross talk in Alzheimer's disease and Parkinson's disease. *Drug Des., Dev. Ther. 11*, 797−810.

(7) Glass, C. K., Saijo, K., Winner, B., Marchetto, M. C., and Gage, F. H. (2010) Mechanisms underlying inflammation in neurodegeneration. *Cell 140*, 918−934.

(8) Mach, R. H. (2014) New targets for the development of PET tracers for imaging neurodegeneration in Alzheimer disease. *J. Nucl. Med. 55*, 1221−1224.

(9) Gomes, A., Fernandes, E., and Lima, J. L. F. C. (2005) Fluorescence probes used for detection of reactive oxygen species. *J. Biochem. Biophys. Methods 65*, 45−80.

(10) Dugan, L. L., and Quick, K. L. (2005) Reactive oxygen species and aging: evolving questions. *Science of Aging Knowledge Environment 2005*, pe20.

(11) Dugan, L. L., Ali, S. S., Shekhtman, G., Roberts, A. J., Lucero, J., Quick, K. L., and Behrens, M. M. (2009) IL-6 mediated degeneration of forebrain GABAergic interneurons and cognitive impairment in aged mice through activation of neuronal NADPH oxidase. *PLoS One 4*, No. e5518.

(12) Chu, W., Chepetan, A., Zhou, D., Shoghi, K. I., Xu, J., Dugan, L. L., Gropler, R. J., Mintun, M. A., and Mach, R. H. (2014) Development of a PET radiotracer for non-invasive imaging of the reactive oxygen species, superoxide, in vivo. *Org. Biomol. Chem. 12*, 4421−4431.

(13) Hall, D. J., Han, S. H., Chepetan, A., Inui, E. G., Rogers, M., and Dugan, L. L. (2012) Dynamic optical imaging of metabolic and NADPH oxidase-derived superoxide in live mouse brain using fluorescence lifetime unmixing. *J. Cereb. Blood Flow Metab. 32*, 23−32.

(14) Carstens, E., and Moberg, G. P. (2000) Recognizing Pain and Distress in Laboratory Animals. *ILAR J. 41*, 62−71.

(15) Graeber, M. B. (2010) Changing face of microglia. *Science (Washington, DC, U. S.) 330*, 783−788.

(16) Carroll, V., Michel, B. W., Blecha, J., VanBrocklin, H., Keshari, K., Wilson, D., and Chang, C. J. (2014) A boronate-caged [(1)(8)F]FLT probe for hydrogen peroxide detection using positron emission tomography. *J. Am. Chem. Soc. 136*, 14742−14745.

(17) Carroll, V. N., Truillet, C., Shen, B., Flavell, R. R., Shao, X., Evans, M. J., VanBrocklin, H. F., Scott, P. J., Chin, F. T., and Wilson, D. M. (2016) [(11)C]Ascorbic and [(11)C]dehydroascorbic acid, an endogenous redox pair for sensing reactive oxygen species using positron emission tomography. *Chem. Commun. (Cambridge, U. K.) 52*, 4888−4890.

(18) Al-Karmi, S., Albu, S. A., Vito, A., Janzen, N., Czorny, S., Banevicius, L., Nanao, M., Zubieta, J., Capretta, A., and Valliant, J. F. (2017) Preparation of an 18 F-Labeled Hydrocyanine Dye as a Multimodal Probe for Reactive Oxygen Species. *Chem. - Eur. J. 23*, 254−258.

(19) Yang, H., Jenni, S., Colovic, M., Merkens, H., Poleschuk, C., Rodrigo, I., Miao, Q., Johnson, B. F., Rishel, M. J., Sossi, V., Webster, J. M., Benard, F., and Schaffer, P. (2017) 18F-5-Fluoroaminosuberic Acid as a Potential Tracer to Gauge Oxidative Stress in Breast Cancer Models. *J. Nucl. Med. 58*, 367−373.

(20) Okamura, T., Okada, M., Kikuchi, T., Wakizaka, H., and Zhang, M. R. (2015) A (1)(1)C-labeled 1,4-dihydroquinoline derivative as a potential PET tracer for imaging of redox status in mouse brain,. *J. Cereb. Blood Flow Metab. 35*, 1930−1936.

(21) Abe, K., Takai, N., Fukumoto, K., Imamoto, N., Tonomura, M., Ito, M., Kanegawa, N., Sakai, K., Morimoto, K., Todoroki, K., and Inoue, O. (2014) In vivo imaging of reactive oxygen species in mouse brain by using [3H]hydromethidine as a potential radical trapping radiotracer. *J. Cereb. Blood Flow Metab. 34*, 1907−1913.

(22) Wilson, A. A., Sadovski, O., Nobrega, J. N., Raymond, R. J., Bambico, F. R., Nashed, M. G., Garcia, A., Bloomfield, P. M., Houle, S., Mizrahi, R., and Tong, J. (2017) Evaluation of a novel radiotracer for positron emission tomography imaging of reactive oxygen species in the central nervous system. *Nucl. Med. Biol. 53*, 14−20.

(23) Takai, N., Abe, K., Tonomura, M., Imamoto, N., Fukumoto, K., Ito, M., Momosaki, S., Fujisawa, K., Morimoto, K., Takasu, N., and Inoue, O. (2015) Imaging of reactive oxygen species using [(3)H]hydromethidine in mice with cisplatin-induced nephrotoxicity. *EJNMMI Res. 5*, 116.

(24) Abe, K., Tonomura, M., Ito, M., Takai, N., Imamoto, N., Rokugawa, T., Momosaki, S., Fukumoto, K., Morimoto, K., and Inoue, O. (2015) Imaging of reactive oxygen species in focal ischemic mouse brain using a radical trapping tracer [(3)H]hydromethidine. *EJNMMI Res. 5*, 115.

DOI: 10.1021/acschemneuro.7b00385
ACS Chem. Neurosci. 2018, 9, 578−586